NUREG/CR-0219
LA-7387-SR

Status Report

A Numerical Study of Apparatus Scaling in a Pressurized Water Reactor

A Status Report—May 1978

University of California

LOS ALAMOS SCIENTIFIC LABORATORY
Post Office Box 1663 Los Alamos, New Mexico 87545

NUREG/CR-0219
LA-7387-SR
Status Report
R-4

A Numerical Study of Apparatus Scaling in a Pressurized Water Reactor

A Status Report—May 1978

B. J. Daly

Manuscript submitted: June 1978
Date published: July 1978

Prepared for
Division of Reactor Safety Research
Office of Nuclear Regulatory Research
US Nuclear Regulatory Commission
Washington, DC 20555

NRC FIN No. A-7027-8

UNITED STATES
DEPARTMENT OF ENERGY
CONTRACT W-7405-ENG. 36

A NUMERICAL STUDY OF APPARATUS SCALING IN A PRESSURIZED WATER REACTOR

A Status Report--May 1978

by

B. J. Daly

ABSTRACT

The K-TIF numerical method for calculating the transient dynamics of two interpenetrating fluids has been extended and applied to the study of scaling of the downcomer and lower plenum regions of a pressurized water reactor during a hypothetical loss of coolant accident. Tentative criteria are established for judging the similarity of flows at different apparatus scales. These criteria are used to evaluate various procedures for specifying inflow velocities of the time varying steam flow from the reactor core and the emergency core coolant supply to determine the most appropriate procedure for modeling full scale phenomena with small scale experiments. The sensitivity of scaling relationships to lower plenum pressure levels is examined by comparing results obtained at pressures that are typical of small - scale experiments with those at higher pressures. Sensitivity studies are also performed to determine the importance of various properties of the theoretical model and the numerical calculation procedure.

I. INTRODUCTION

An extensive series of experiments at 1/30,[1] 1/15,[2-4] and 2/15[4-5] scales have been performed to investigate steam-water interactions during the bypass and refill stages of a hypothetical loss of coolant accident (LOCA) in a pressurized water reactor (PWR). These experiments have examined a wide variety of factors that might influence the mass, momentum, and heat exchange between the phases and with the confining walls. The purpose of these experimental studies has been to determine the effectiveness of the emergency core coolant (ECC) system in refilling the lower plenum and reflooding the reactor core with water.

The usefulness of these experimental results depends upon the development of the proper scaling relationships by which small-scale experiments can be extrapolated to full scale. In this study, we make use of a numerical method for calculating the transient dynamics of two interpenetrating fluids to examine the effects of apparatus scale size on steam-water interactions in the downcomer and on ECC delivery. The results of these numerical calculations can be used to interpret existing small-scale experimental data in terms of the full-scale reactor and to propose relevant future experiments. In addition, this study demonstrates the capability of examining flow variations at full scale to provide guidance for PWR licensing.

To relate small-scale results to the full-scale reactor, some criterion must be established for describing flow similarity at different scales. Two criteria have been established in the present study: the per cent of injected water that is delivered to the lower plenum when the lower plenum is 90% full should be similar at the various scales, and the stage of flow development attained prior to the onset of delivery to the lower plenum should be the same at all scales. The latter criterion is illustrated by examples.

The procedure that is used to specify the inflow velocity of the steam and the water at different scales has important consequences for flow similarity. Several types of inflow specifications are considered in this study and an optimum procedure is suggested. The sensitivity of scaling relationships to lower plenum pressure levels is tested by comparing results obtained at lower plenum pressures that can be achieved in small-scale experiments with those obtained using pressures that are more typical of a full-scale reactor. The effect of water boiling in the lower plenum is examined by initiating a calculation with the lower plenum partially filled with water at saturation temperature. In addition, a series of calculations has been performed to test the sensitivity of results to the various properties of the numerical model. The modeling variations examined include the procedure for specifying the liquid and gas entity sizes used in the momentum exchange function, the equation used in computing the heat diffusion through the confining walls, the neglect of the three dimensionality of the lower plenum, and the finite difference mesh resolution.

II. THE PHYSICAL MODEL

The flow model described here is an extension of the K-TIF finite difference procedure proposed by Amsden and Harlow.[6] The reader is referred to that reference for a more detailed description.

It is assumed in this study that sound velocity is much greater than material velocity so that microscopic density is independent of position. However, the effect of temporal variations in gas density as a result of overall compression or expansion of the fluid is included. With these considerations, the mass conservation equations can be written

$$\frac{\partial \theta_1}{\partial t} + \nabla \cdot (\theta_1 \vec{u}_1) = - J/\rho_1 - S_1 \quad , \tag{1}$$

$$\frac{\partial \theta_2}{\partial t} + \nabla \cdot (\theta_2 \vec{u}_2) = + J/\rho_2 - S_2 - \frac{\theta_2}{\rho_2} \frac{d\rho_2}{dt} \quad . \tag{2}$$

The subscripts 1 and 2 refer to water and gas, respectively; θ is volume fraction, u is velocity, ρ is microscopic density, J is the mass per unit volume per unit time changing phase and S is the volume per unit volume per unit time entering or leaving the system.

The steam is assumed to be always at the saturation temperature, T_s. Accordingly, the phase change model is written

$$J = J_L \, \theta_{eff} \, (T_1 - T_s)/T_s \quad , \tag{3}$$

where T is temperature and

$$\theta_{eff} = \begin{cases} \theta_1 \text{ if } T_1 > T_s \text{ (evaporation)} \\ \theta_1 \, \theta_2 \, \alpha \text{ if } T_1 < T_s \text{ (condensation)} \end{cases} \tag{4}$$

Here α is the fraction of the gas volume that is steam, the remainder being air. The form for θ_{eff} in Eq. (4) is changed from that proposed in Ref. 6. The present form reflects the fact that evaporation can take place in the absence of steam (there being an abundance of nucleation sites in this turbulently mixed flow), but that condensation requires the movement of cool water to the phase

transition interface where water and steam exist in equilibrium. Condensation then takes place to the extent allowed by the release of latent heat and the consequent heating of the water.

Air can enter the system through the broken water supply pipe if the pressure in the downcomer drops below the external pressure as a result of condensation in the downcomer. This air is then convected throughout the downcomer and lower plenum with the gas velocity. Its presence can affect condensation locally by occupying volume that would otherwise be occupied by steam. However, in the highly mixed, turbulent flow that we are considering, it is assumed that the gas components are sufficiently well mixed that the available steam can come into contact with the water.

Another modification of K-TIF has been to compute phase change in the ECC inlet cells. In earlier versions of K-TIF this was not done. The effect of this change has been to increase mass and momentum exchange through condensation. These changes should prolong holdup.

The coefficient J_L in Eq. (3) is a negative constant in the calculations reported here, but an anticipated extension is to relate J_L to the magnitude of the local turbulent mixing rate.

The momentum equations for this two-phase flow are written

$$\frac{\partial(\theta_1 \vec{u}_1)}{\partial t} + \nabla \cdot (\theta_1 \vec{u}_1 \vec{u}_1) = - \frac{\theta_1}{\rho_1} \nabla p + \theta_1 \vec{g} + \frac{K}{\rho_1} (\vec{u}_2 - \vec{u}_1) + \nu_{T1} (\nabla \cdot \theta_1 \nabla) \vec{u}_1 - \frac{J}{2\rho_1} [(1 + \text{sign } J) \vec{u}_1 + (1 - \text{sign } J) \vec{u}_2] , \quad (5)$$

$$\frac{\partial(\theta_2 \vec{u}_2)}{\partial t} + \nabla \cdot (\theta_2 \vec{u}_2 \vec{u}_2) = - \frac{\theta_2}{\rho_2} \nabla p + \theta_2 \vec{g} + \frac{K}{\rho_2} (\vec{u}_1 - \vec{u}_2) + \nu_{T2} (\nabla \cdot \theta_2 \nabla) \vec{u}_2 + \frac{J}{2\rho_2} [(1 + \text{sign } J) \vec{u}_1 + (1 - \text{sign } J) \vec{u}_2] - \frac{\theta_2 \vec{u}_2}{\rho_2} \frac{d\rho_2}{dt} , \quad (6)$$

where p is the pressure, $\vec{g}$ is the gravitational acceleration, ν_T is the kinematic eddy viscosity coefficient and

$$\text{sign } J = \begin{cases} +1 \text{ for } J > 0 \\ -1 \text{ for } J < 0 \end{cases} .$$

The momentum exchange function K has the form

$$K = \frac{3}{8}(r_1 + r_2)^2 \left(\frac{C_D \rho_1 \theta_1 \rho_2 \theta_2}{r_1 r_2}\right)\left(\frac{|\vec{u}_1 - \vec{u}_2|}{r_2 \rho_1 + r_1 \rho_2}\right) , \tag{7}$$

where r is entity size and C_D is the drag coefficient. If $\theta_2 < 0.1$, K is set to a large value with the effect that the gas then moves with the liquid. With this provision the K formulation in Eq. (7) reduces to the appropriate limits for small θ_1 and small θ_2, and is intended to be appropriate for intermediate values. This momentum exchange function was proposed by Harlow and Amsden[7] on the basis of available momentum arguments. It has previously been applied in comparisons with countercurrent air-water experiments.[8] A discussion of the choice of entity size is presented in the following section.

In the present version of K-TIF the momentum exchange function, K, is evaluated at the mesh cell faces, whereas in earlier versions of K-TIF, K was evaluated at cell centers and then averaged to obtain the cell face values. By avoiding this averaging procedure the current model incorporates a more locally determined and generally enhanced momentum exchange. One effect of this change should be a greater delay in the onset of ECC delivery to the lower plenum than was observed in previous comparisons with experiment.[10]

With the assumption that the steam is always at saturation temperature, only a transport equation for water temperature is required,

$$\frac{\partial T_1 \theta_1}{\partial t} + \nabla \cdot (T_1 \theta_1 \vec{u}_1) + \frac{J T_s}{\rho_1} = -\frac{Q}{\rho_1 b_1} J + \frac{z\, k_w\, (T_{dw} - T_s)}{\rho_1\, b_1\, s\, \gamma} . \tag{8}$$

Here Q is the specific latent heat of vaporization, b_1 is the specific heat of the water, z is the number of walls adjacent to the water, k_w is the thermal conductivity of the wall, T_{dw} is the deep interior wall temperature, s is the downcomer gap width and γ measures the depth of penetration of a heating or

cooling wave into the wall. We assume in Eq. (8) that the wall edge is at saturation temperature rather than the water temperature as in Ref. 6 when water is adjacent to the wall. This change will generally decrease the heat transfer from the wall, and thereby enhance momentum transfer through condensation. The result should be prolonged water holdup. The presence of the downcomer gap width, s, in the denominator of the heat flux term in Eq. (8) ensures that the effect of wall heat flux is diminshed as the system scale size is increased.

An equation for the depth of penetration, γ, is obtained by assuming that a solution to the wall heat diffusion equation,

$$\frac{\partial T_w}{\partial t} + K_w \frac{\partial^2 T_w}{\partial \xi^2} = 0 \quad , \tag{9}$$

can be expressed in terms of the similarity function,

$$\eta = \xi / \left(2 \sqrt{K_w t} \right) . \tag{10}$$

Here, T_w is the wall temperature, ξ is distance from the wall edge and K_w is the thermometric conductivity. The solution to Eq. (9), subject to the appropriate boundary conditions, is

$$T_w = T_{dw} + (T_s - T_{dw}) \left[1 - \frac{2}{\sqrt{\pi}} \operatorname{erf}(\eta) \right] . \tag{11}$$

We choose γ to be that value of ξ at which $T_w = .9\, T_{dw} + .1\, T_s$. This occurs when $\eta \approx 1.0$ or $\gamma = 2 \sqrt{K_w t}$. From this we obtain an equation for the time variation of γ^2,

$$\frac{\partial \gamma^2}{\partial t} = 4 K_w . \tag{12}$$

In the original version of K-TIF,[6] Eq. (12) was written,

$$\frac{\partial \gamma^2}{\partial t} = K_w . \tag{13}$$

The use of Eq. (12) permits a more rapid penetration of a cooling wave into the wall. This decreases the heat transfer from the wall to the water and conse-

quently increases the mass and momentum exchange through condensation. The effect of this change is examined below.

III. CHARACTERISTIC ENTITY SIZE

Some guidance regarding the variation of entity size with scale can be obtained from empirical counter-current air-water flow correlations and the balance of forces concepts upon which they are based. At equilibrium, the balance between buoyancy and drag forces acting over a single spherical drop can be written,

$$C_D \; 1/2 \; \rho_2 \; (\vec{u}_1 - \vec{u}_2)^2 \; \pi r^2 = |\vec{g}| \; (\rho_1 - \rho_2) \; 4/3 \; \pi r^3 \quad ,$$

where r is the drop radius. If the average drop velocity is zero, the dimensionful quantities can be grouped to give

$$\frac{\rho_2 \; u_2^2}{|\vec{g}| \; 2r(\rho_1 - \rho_2)} = \frac{4}{3C_D} \quad , \tag{14}$$

where $\vec{u}_2$ is the minimum gas velocity required to prevent water penetration. The Wallis[9] and Kutateladze[9] correlations for zero water penetration differ in the manner of modeling the droplet diameter, 2r. Richter and Lovell[9] found, when this entity size was assumed to scale in proportion to the pipe size, that the left hand side of Eq. (14) remained approximately constant for pipes with diameters less than two inches. This is the Wallis correlation. However, this correlation breaks down at larger pipe sizes, indicating a limit to the importance of boundary effects on entity size.

For pipe sizes larger than 2 inches they found that the zero penetration data could best be correlated by using the Kutateladze correlation,

$$2r = \left[\frac{\sigma}{g(\rho_1 - \rho_2)} \right]^{1/2} = 0.11 \text{ in. for air-water} \quad , \tag{15}$$

where σ is the surface tension coefficient. This form can be obtained by balancing surface tension and drag forces and using Eq. (14). Then

$$r^2 = 3/8\ C_D\ We\ \frac{\sigma}{g(\rho_1 - \rho_2)} \quad , \tag{16}$$

where We is the Weber number for an isolated drop. Equations (15) and (16) are equivalent when $C_D We = 0.67$. In the numerical study we obtain the best agreement with experiment when $C_D = 0.6$, so that We = 1.1 is consistent with the Kutateladze entity size expression. Indeed, in the numerical calculations we have found that the use of a critical Weber number formulation for r, $r = We\ \sigma/[\rho_2(\vec{u}_1 - \vec{u}_2)^2]$, with We = 1.1, or the use of a constant value, r = 0.06 in. [in good agreement with Eq. (15)], gives the best and essentially the same results.

Substituting Eq. (15) into Eq. (14), one can obtain the form of the Kutateladze correlation,

$$\frac{\rho_2^{1/2}|\vec{u}_2|}{[g\ \sigma(\rho_1 - \rho_2)]^{1/4}} = \left(\frac{8}{3}\ \frac{We}{C_D}\right)^{1/4} \quad . \tag{17}$$

Evaluating the right hand side of Eq. (17) with the values used in the numerical calculations gives a value of 1.5. In the Kutateladze correlation for pipes the value of the right hand side of Eq. (17) is generally found to be approximately 3.0.[9] This quantitative discrepancy is quite acceptable in view of the differences in geometry between calculation and experiment as well as the heuristic arguments leading to Eq. (17).

IV. APPLICATION OF THE METHOD

A. Comparisons with 1/15 and 2/15-Scale Models of a PWR

The K-TIF code has been used to calculate a series of transient steam water flows[10] for comparison with specific experiments[2] performed by Creare, Inc. in a 1/15th scale model of a pressurized water reactor. A comparison of the calculated and experimental measurements of the time delay and rate of delivery of water from the downcomer to the lower plenum showed a consistent trend for a variety of water injection rates and subcoolings, steam flow and pressure ramp rates and wall superheat. In all cases the numerical calculations predicted a shorter delay time for the onset of water delivery to the lower plenum than was measured in the experiments.

As discussed above, the K-TIF model used in that comparison has since been extended by several modifications (e.g., the inclusion of an air component in the gas field and a more local determination of the momentum exchange function, K) that tend to prolong the delay time for water delivery. This extended version of K-TIF has been used to simulate a transient flow experiment performed in a 2/15 scale model of a PWR by Battelle Columbus Laboratories.[5] Figure 1 shows the computation mesh used in that numerical calculation. For display purposes the downcomer annulus is pictured as unwrapped. In the calculations the flow is resolved in the azimuthal (horizontal) and vertical directions, but flow variations across the downcomer gap are not resolved. The left and right boundaries of the mesh are connected while the top is a free-slip boundary. The bottom is a prescribed inflow boundary for the time-varying steam flow from the lower plenum and a continuative outflow boundary for the water and the gas. The deep lower plenum used in the experiment is not resolved in the calculations.

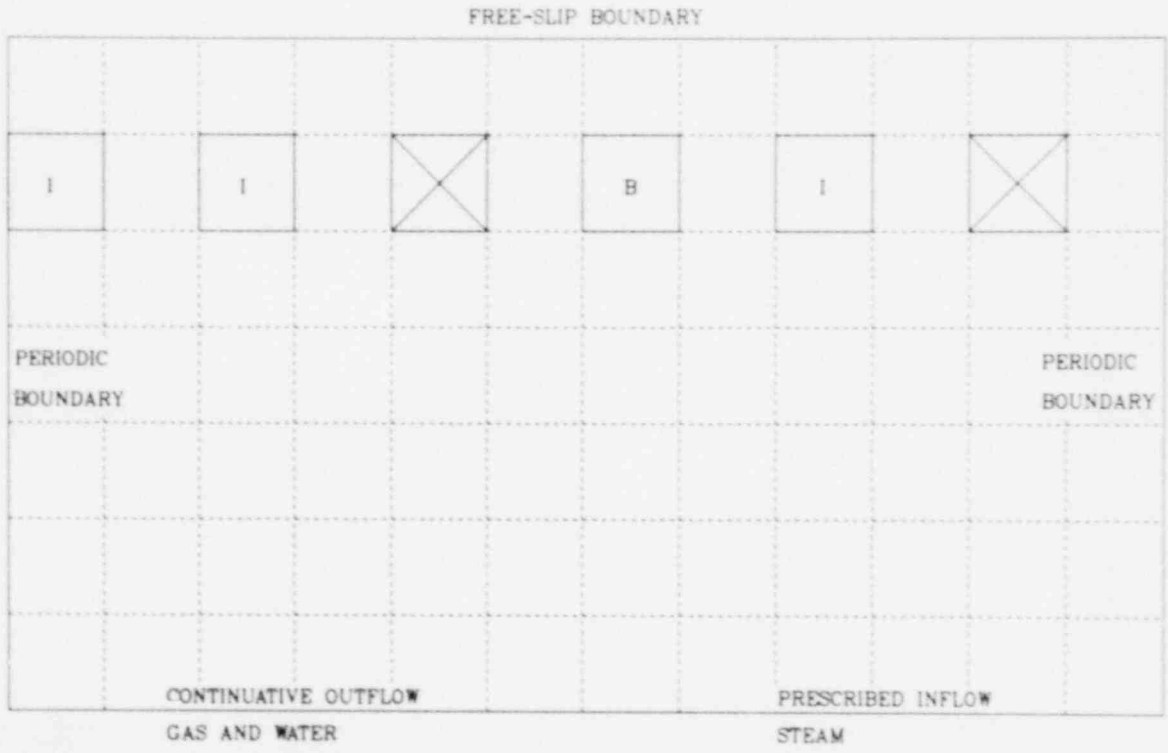

Fig. 1. Computation mesh and boundary conditions used in flow comparison with 2/15 scale experiment by Battelle Columbus Laboratories. The cells labeled I near the top of the mesh represent intact inlet pipes for coolant water. The cell labeled B represents a broken inlet pipe.

Emergency core coolant enters the downcomer through the three intact cold water injection ports, labeled I, near the top of the mesh. Water and gas (steam and air) can leave the downcomer through the broken cold water pipe, labeled B. However, if the pressure in the downcomer falls below ambient as a result of condensation, so that there is flow into the downcomer through the broken leg, then the fluid flowing into the system is air. The two cross-hatched mesh cells near the top of the mesh simulate hot legs connecting the core with the external power generating equipment. These are treated as obstacles in the numerical calculation.

In the Battelle experiment, 93 K (168°F) subcooled water is injected at the rate of 407 gallons per minute through the three intact cold legs. The time-varying steam flow and lower plenum pressure are shown in Fig. 2. The core barrel and vessel walls are at the initial saturation temperature, 424 K (303°F).

The numerical calculation of this experiment makes use of a computation grid (Fig. 1) of square cells, 6.05 inches on a side, with 12 cells in the horizontal direction and 7 cells in the vertical direction. The water injection rate corresponds to that of the experiment, but the steam flow ramp rate and the pressure transient used in the calculation are smooth representations of the curves shown in Fig. 2.

Figure 2 also shows a comparison of the measured and calculated lower plenum filling curves as they vary in time. The experimental liquid level is measured at discrete sensing positions, giving rise to a stair-step appearance to the curve. The calculated liquid level is obtained by computing the total volume of water crossing the bottom boundary of the downcomer and dividing by the cross sectional area of the lower plenum. The two curves are in satisfactory agreement regarding the delay time for the onset of water delivery to the lower plenum, and in good agreement regarding the rate of delivery.

B. Sensitivity to Apparatus Scale Size

A series of K-TIF calculations has been performed in order to investigate the sensitivity of the flow dynamics at different apparatus scales to the water and steam inflow boundary condition scaling. It should be emphasized that the results to be presented here are preliminary and that much additional work remains to be done before a full understanding of flow variations with apparatus scale is obtained. The tentative nature of the present results derives from several considerations:

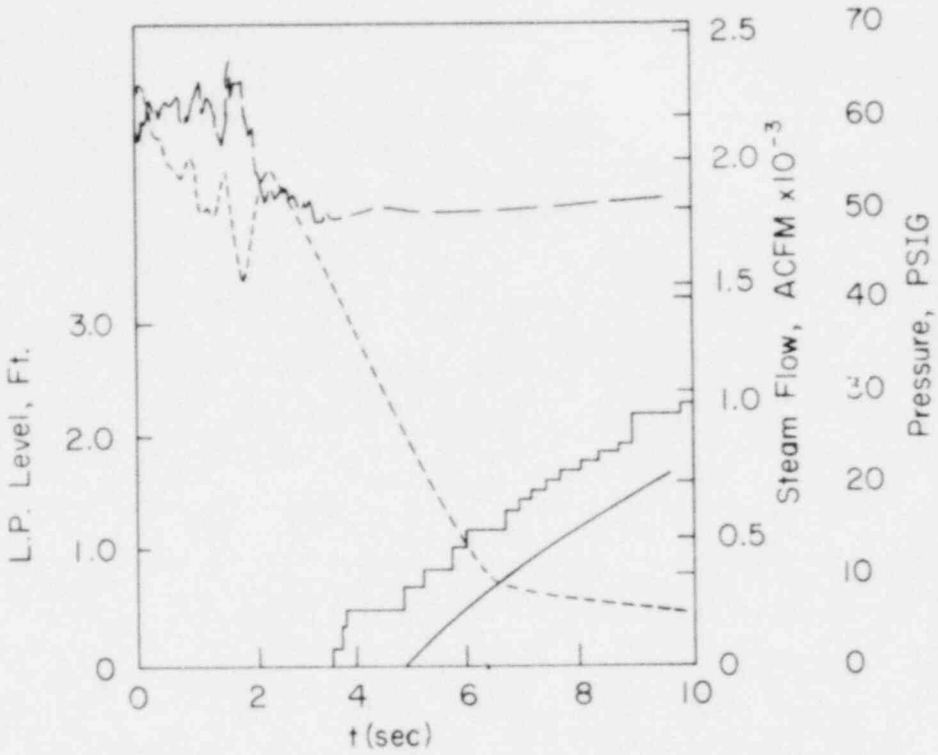

Fig. 2. The transient steam flow (---) and lower plenum pressure (– –) measured by Battelle Columbus Laboratories in a 2/15 scale model experiment, representing a hypothetical loss of coolant accident in a PWR. The solid lines indicate the experimental (stair-step curve) and calculated lower plenum filling curves.

1. The lack of flow representation in the radial direction, the consequences of which could vary with scale.

2. Uncertainties regarding the constitutive relations. For example, the mass exchange function, Eq. (3), does not take into account the turbulent nature of the flow in the downcomer, which must have an important effect upon the details of interphase mixing. The momentum exchange function, Eq. (7), is novel and has not yet been sufficiently tested for simpler flow conditions.

3. While the flow model described here has been shown to give results that are consistent with small-scale experiments for many flow conditions,[10] quantitative agreement has not yet been demonstrated for a wide spectrum of flow variations.

4. Some of the parameter variations considered in the following study have not previously been tested in small-scale comparisons.

With these reservations in mind, let us examine the trends indicated in these numerical calculations regarding the similarity of flow development at 2/15, 1/2, and full scales. We shall describe flow similarity at different scales according to two criteria:

1. Agreement in the per cent of injected water that has been delivered to the lower plenum when the lower plenum is 90% full. This is an important criterion since it measures the effectiveness of the emergency core coolant supply system at full scale. The ultimate usefulness of small-scale experiments rests on their ability to accurately predict the percentage.

2. Close similarity in fluid configuration at the onset of water delivery to the lower plenum. It has been observed in these calculations that the distribution and dynamics of water flow in the downcomer develops in three stages, as illustrated in Fig. 3. In the initial stage the water that is injected into the downcomer accumulates as single large entities, or "globs." This water is then entrained in the second stage by the upward directed steam flow and set in a swirling motion in the region above the inlet legs. Because of a favorable pressure gradient, part of this swirling water bypasses the system through the broken inlet leg. In the final stage of flow development, sufficient water accumulates below the intact cold legs that momentum transfer from the steam produces bypass from below the broken leg.

Depending on the inflow conditions, some flows may not proceed beyond the first or the second stage of this development. For example, if the water injection rate is small the local overpressure resulting from the inflow will also be small. Hence there will be little spreading of the water interface, so that the area of contact between the phases will remain small and little momentum transfer will take place unless the steam flow rate is large. The water will then fall into the lower plenum as two isolated streams below the injection legs. With somewhat more spreading or increased

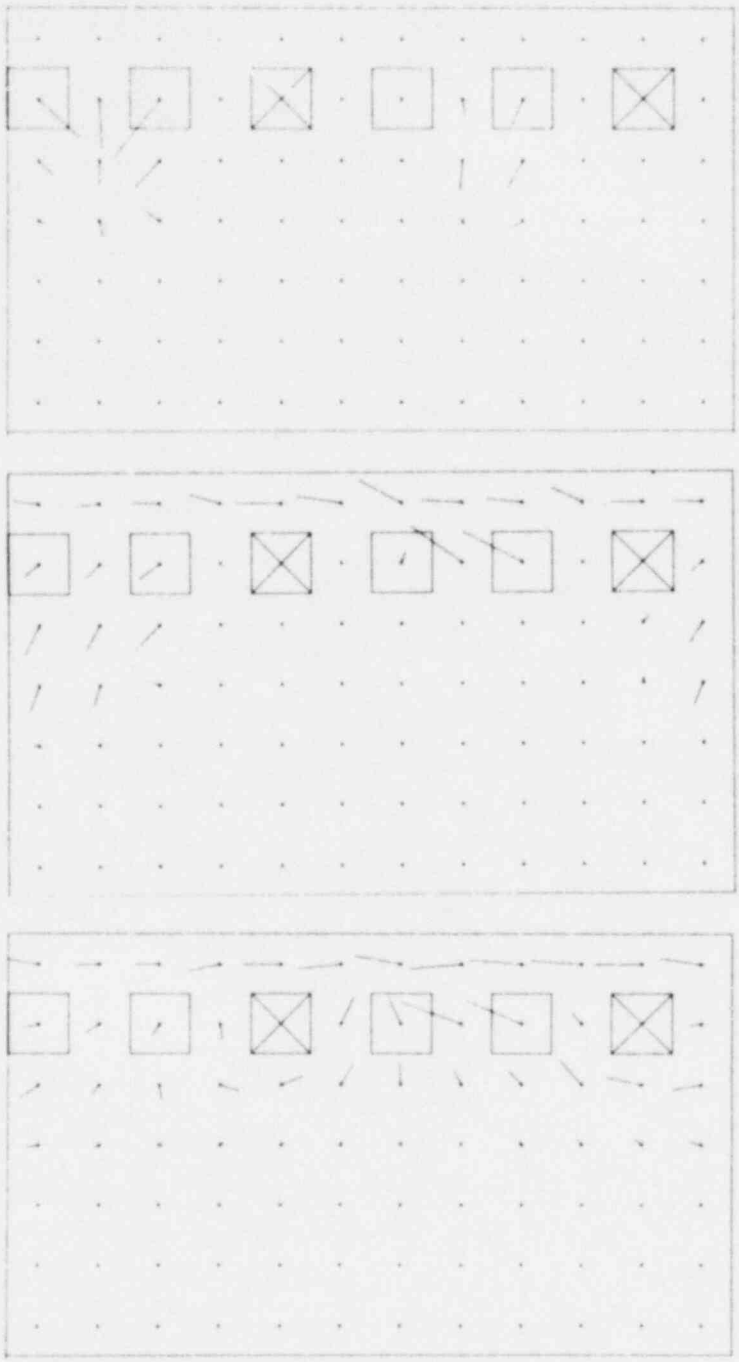

Fig. 3. Water volume flow plots showing three stages in flow development prior to the onset of water delivery to the lower plenum. Top. The injected water accumulates below the inlet legs. Middle. As a result of momentum transfer from the steam, the water is set in a swirling motion in the region above the inlet legs. Bottom. Additional momentum transfer produces water bypass from below the broken leg.

steam flow the momentum transfer may be sufficient to give rise to the swirling flow development. Delivery to the lower plenum then occurs as a single, rapidly falling water stream. As the momentum transfer is increased even more, bypass may occur from below the broken leg as indicated in Fig. 3. The increased contact area between the phases results in increased momentum transfer through condensation and interfacial drag. Water delivery to the lower plenum is thereby delayed.

The second criterion that we have used in defining flow similarity is that the flows have reached the same stage of flow development before the onset of water delivery to the lower plenum. The reasonableness of this criterion for flow similarity rests on the observation that the timing and nature of flow delivery from the downcomer to the lower plenum varies greatly depending upon the stage of flow development that has been reached. Therefore, if small-scale experiments are to be an accurate representation of full-scale events, it would appear to be important that the two flows have reached the same stage of flow development before delivery to the lower plenum.

Calculations were performed at 2/15, 1/2, and full scales using the calculation mesh shown in Fig. 4. In these calculations the lower plenum is explicitly resolved as a linear extension of the downcomer with the appropriate volume. Boundary conditions are identical to those described for Fig. 1, except that steam is now injected throughout the entire lower plenum rather than being prescribed at the boundary between the downcomer and the lower plenum, and the bottom boundary condition now represents a free-slip rigid wall.

Table I summarizes the test conditions and some of the results of these transient calculations. In all cases the lower plenum pressure and the steam injection velocity, j_g, were linearly ramped from their initial values to their final values in 10 seconds. The water injection velocity, j_L, is a specified constant in any calculation. These injection velocities are determined from the volume rate of flow into the downcomer divided by the downcomer cross sectional area. The column headed t_{DELAY} gives the delay time for the onset of water delivery to the lower plenum. The last two columns provide a measure of the flow similarity criteria described above. The first of these is the per cent of injected water that is delivered to the lower plenum when it is 90% full. The final column gives the stage of

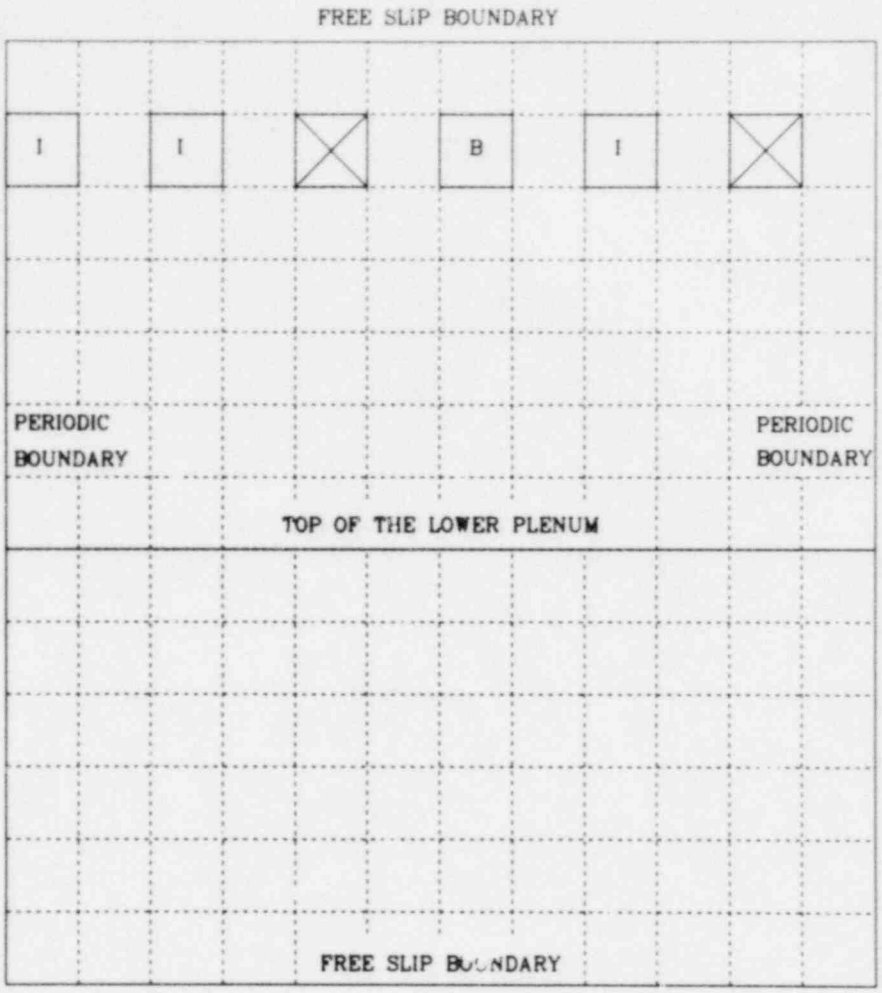

Fig. 4. Computation mesh and boundary conditions used in the transient flow comparisons at 2/15, 1/2, and full scales. In these calculations steam was injected throughout those parts of the lower plenum that were not occupied by water.

flow development just prior to delivery to the lower plenum, 1 corresponding to almost immediate delivery as two isolated streams below the injection legs, 2 being the development of swirling flow above the injection legs followed by delivery as a single stream without any bypass from below the broken leg, and 3 being the development of bypass from below the broken leg before delivery. A flow regime, 2-3, is a borderline case in which there is only a slight amount of bypass from below the broken leg before delivery.

TABLE I

TEST CONDITIONS AND RESULTS

Run	Scale	LP Pressure PSIA t = 0/t ≥ 10	j_g in/sec t = 0/t > 10	j_L in/sec	t_{Delay} sec	% Delivered 90% Full	Flow Regime
1	1	175/60	611/0	22.5	2.6	90	1
2	1/2	175/60	611/0	22.5	2.5	75	2
3	2/15	175/60	611/0	22.5	4.3	24	3
4[1]	1	175/60	611/0	22.5	2.9	95	1
5[1]	1/2	175/60	611/0	22.5	2.5	79	2
6[1]	2/15	175/60	611/0	22.5	4.6	NA	3
7	1	175/70	4583/0	168.5	8.5	7	3
8	1/2	175/60	2291/0	84.3	7.6	15	3
9	1	175/60	1674/0	61.5	4.3	44	2-3
10	1/2	175/60	1674/0	61.5	6.3	24	3
11	2/15	175/60	1674/0	61.5	7.5	6	3
12	1/2	175/60	837/0	30.8	4.6	55	2
13	2/15	175/60	223/0	8.2	0.7	90	1
14	1/2	175/60	1183/0	43.5	6.1	30	3
15	1/2	175/60	1674/0	30.8	6.2	40	3
16	2/15	175/60	1674/0	8.2	8.5	37	3
17[2]	1	175/60	1674/0	61.5	3.6	NA	2-3
18[1]	1	175/60	1674/0	61.5	3.8	44	2-3
19[1]	1/2	175/60	1674/0	30.8	6.5	40	3
20[1]	2/15	175/60	1674/0	8.2	8.6	36	3
21[3]	1	175/60	1674/0	61.5	3.5	48	2-3
22[4]	1/2	175/60	1674/0	30.8	6.3	44	3
23[5]	1	175/60	1674/0	61.5	4.3	43	2-3
24[5]	1/2	175/60	1674/0	30.8	6.2	39	3
25[6]	1	175/60	1674/0	61.5	5.0	40	3
26[7]	1	175/60	1674/0	61.5	6.3	7	3
27	1	75/15	1655/0	61.5	2.9	61	2
28	1/2	75/15	1655/0	30.8	3.3	59	2
29	2/15	75/15	1655/0	8.2	--	0	3
30[8]	1	75/15	1655/0	61.5	3.1	60	2
31[8]	2/15	75/15	1655/0	8.2	--	0	3

1 - Weber number formulation for r.
2 - Double the standard mesh resolution.
3 - r = 0.45 in. (constant).
4 - r = 0.225 in. (constant).
5 - Using Eq. (12).
6 - LP 1/3 full of water initially.
7 - Only one row of mesh cells in LP.
8 - Superheated walls.

Except where otherwise noted, the parameter values used in these calculations are those shown in Table II. Also, except where noted, Eq. (13) is used to calculate the depth of penetration of a cooling wave into the wall.

Inflow Boundary Conditions: Effect on Flow Similarity. Figures 5-8 show plots of water delivered to the lower plenum and bypassed through the broken leg as percentages of the total water injected up to that time for various types of inflow boundary specification. The results shown at full scale are from the same calculation in all four plots. The water and steam inflow specification used in that calculation are obtained from a system calculation of a hypothetical loss of coolant accident in a Combustion Engineering System 80 reactor.

The purpose of these comparisons is to determine which type of inflow specification results in small-scale results that are similar to full-scale in the sense described above, i.e., that have the same per cent of injected water delivered to the lower plenum when the lower plenum is 90% full, and that have reached the same stage of flow development before delivery to the lower plenum. The latter criterion is not satisfied in the case shown in Fig. 6, for which the water and steam inflow velocities are proportional

TABLE II

PARAMETER VALUES

Mean Downcomer Circumference: 541.2" x Scale

Downcomer Height: 315.7" x Scale

Downcomer Gap: 10" x Scale

Lower Plenum Height: 270.6" x Scale

Computation Cell Edge: 45.1" x Scale

Entity Size: $r_1 = r_2 = 0.06$" (constant)

Drag Coefficient: $C_D = 0.6$

Phase Change Coefficient: $J_L = -0.16$ lb/(in^2 x sec)

ECC Temperature: $T_{ECC} = 120°F = 322°K$

Deep Wall Temperature: $T_{dw} = T_s(t = 0)$

to scale. In that case the 2/15 scale calculation did not develop beyond the first stage of flow development, while the 1/2 scale calculation reached the second stage of development. The full-scale calculation shown in Figs. 5-8 only reached the third stage of flow development in a marginal sense. There was a small amount of bypass from below the broken leg in this calculation, but it did not develop until the water stream began to fall through the downcomer toward the lower plenum. On the other hand, the 2/15 and 1/2 scale calculations in Figs. 5, 7, and 8 all reached the third stage of flow development prior to the development of the water stream in the downcomer. Thus in these comparisons, the second criterion for flow similarity is only partly satisfied.

The first criterion for similarity of flow at different scales seems to be best satisfied in Fig. 8, in which the inflow velocity of the water is proportional to scale and the inflow velocity of the steam is the same at all scales. Thus at this stage of the numerical scaling study this appears to be the best type of boundary specification.

The results in Figs. 5-8 can be explained in terms of the effect that the various inflow velocity specifications have on the area of contact and the relative velocity between the fluids, and consequently on the mass and momentum exchange. The area of contact between the fluids is influenced to a great extent by the amount of spreading of the inflowing water, and this spreading is in turn related to the local overpressure resulting from the volumetric source of water in that mesh cell. For an incompressible fluid the pressure change in a control volume is proportional to the input rate of volume per unit volume per unit time. If the inflow velocity of the water is proportional to scale, then the overpressure, the spreading and the contact interfacial area will also be proportional to scale. When the contact interface is proportional to scale, the area available for mass and momentum transfer through phase change and fluid drag will be proportional to scale.

It is also important that the relative velocity between the phases be the same at all scales in order that the momentum transfer scale appropriately. The relative velocity within the downcomer is determined from the difference between the inflow velocities of water and steam. However, because the inflow velocity of the steam is many times that of the water, the relative velocity of flow within the downcomer is primarily determined by the inflow velocity of the steam.

Thus, similarity of flow at all scales may require that the inflow velocity of the water be proportional to scale and the inflow velocity of the steam be the same at all scales. These are the conditions that exist for the three calculations of Fig. 8, and these results show a greater similarity of flow at different scale than those of Figs. 5-7.

Reduced Lower Plenum Pressure: Effect on Flow Similarity. Experimental studies in scale models of a PWR are not performed at as high lower plenum pressures as occur in the full-scale apparatus. The peak pressures attained in the Creare and BCL experiments have been approximately 75 psia. As a result of the reduced lower plenum pressure, the steam density and saturation temperatures are also reduced.

We have performed a series of calculations at reduced lower plenum pressure to determine the effect on flow similarity at different scales as well as to examine possible changes in flow development at the same scale. In this series of calculations (runs 27-29 of Table I) we used the standard parameter values of Table II and specified inflow velocities, j_g and j_L, like those of Fig. 8, i.e., j_g constant with scale and ramped to zero in 10 seconds and j_L proportional to scale. The lower plenum pressure was ramped from 75 psia to 15 psia in 10 seconds. Corresponding to this change in lower plenum pressure the gas density decreased from 1.03×10^{-4} lb/in^3 at t = 0 to 2.09×10^{-5} lb/in^3 at t = 10 seconds, and the saturation temperature varied from 425 K to 374 K in the same period. (The corresponding values for the higher pressure calculations, runs 1-26, were 2.39×10^{-4} lb/in^3 and 8.28×10^{-5} lb/in^3 for the steam density, and 460 K and 416 K for the saturation temperature.) As indicated in Table II, the deep interior wall temperature, T_{dw}, is equal to the initial saturation temperature, T_s = 425 K. The temperature of the ECC water, T_{ECC} = 322 K, is unchanged from the higher pressure calculations, so that we have less subcooling in these low pressure runs. It will be seen below that this has considerable effect upon results.

Figure 9 shows plots of water delivered to the lower plenum and bypassed through the broken leg for this series of calculations. Comparing these results with those of Fig. 8, we see that there is a greater per cent of the injected water delivered to the lower plenum at 1/2 and full scales when the lower plenum pressure is reduced, but that no water is delivered to the lower plenum (actually there is a slight amount, less than 1% of in-

jected water) under these conditions at 2/15 scale. Correspondingly, there is less water bypassed at 1/2 and full scales for the reduced lower plenum pressure, while the bypass curve at 2/15 scale is similar in the two figures except that there is no decline in the bypass curve in Fig. 9 as a result of lower plenum delivery.

The change in the pattern of the 1/2 and full-scale curves from those of Fig. 8 can be explained by the fact that there is less momentum exchange between phases as a result of the reduced ECC water subcooling and decreased steam density. As indicated in Table I, both of these calculations were of flow regime 2, meaning that there was no water bypassed from below the broken leg before the onset of delivery to the lower plenum. This delivery occurs as a single stream of water from below the inlet legs furthest from the break. The flow development in these calculations is more similar than that of the 1/2 and full-scale calculations of Fig. 8. This may account for the greater similarity of the delivery curves at 1/2 and full scales in Fig. 9 compared to those of Fig. 8.

The decreased ECC water subcooling and the greater change in T_s of runs 27-29, combined with the increased effect of wall heat transfer at small scale, were the factors that resulted in essentially zero water penetration at 2/15 scale in Fig. 9. The flow development in this calculation was very similar to the 2/15 scale calculation of Fig. 8 up to the onset of water delivery to the lower plenum. At that time the water occupied most of the upper downcomer region above and below the inlet legs. This water was held up by momentum transfer from the steam through condensation, interfacial drag and the development of stagnation pressure. As the steam flow ramped down, the water began to penetrate lower into the downcomer. This advancing water front was subjected to heating by heat transferred from the wall. In the 2/15 scale calculation of Fig. 8, this heating was not sufficient to produce boiling of the water, whereas in the 2/15 scale calculation of Fig. 9 boiling did occur because of greater heat transfer from the wall, as a result of small T_s, and because of decreased ECC subcooling. This boiling along the bottom boundary of the water region was sufficient to hold up the remaining water even after the steam flux from the lower plenum had ramped to zero.

Runs 30 and 31 of Table I were similar to runs 27 and 29 except that the walls in runs 30 and 31 were superheated to 460 K. This had very little effect on results.

Water Initially in the Lower Plenum. A full-scale calculation was performed in which the lower plenum was initially 1/3 full of water to determine the effect on flow development in the downcomer and ECC delivery to the lower plenum. In all other respects this calculation was identical to the full scale calculation of Figs. 5-8. A comparison of the delivery curves for these two calculations is shown in Fig. 10. Except for an initial high level of water bypass as a result of additional steam generation from the boiling of this water in the lower plenum, the curves are similar in appearance. The only effect on water delivery to the lower plenum is a delay of less than one second as a result of the increased momentum transfer from the steam. This increased momentum transfer results in water bypassed from below the broken leg, so that this calculation was of flow regime 3.

Water and Gas Entity Sizes: Sensitivity of Results with Scale. In most of the calculations of this study the water and gas entity sizes, r_1 and r_2, in the momentum exchange function, Eq. (7), have been set to a constant value, 0.06 in. To investigate the sensitivity of results at various scales to variations of this parameter, we have performed two series of experiments. In one series the entity size was made proportional to scale, i.e., $r_1 = r_2 = 0.06$ in. at 2/15 scale, $r_1 = r_2 = 0.225$ in. at 1/2 scale and $r_1 = r_2 = 0.45$ in. at full scale. In the second series of experiments the entity size was determined from a critical Weber number formulation, i.e.,

$$r_1 = r_2 = We \times \sigma/[\rho_2(\vec{u}_1 - \vec{u}_2)^2] \ , \tag{18}$$

where We = 1.1.

Figure 11 shows the delivery and bypass curves that were obtained when the calculations of Fig. 8 were rerun with the entity size proportional to scale. The 2/15 scale results are the same in both figures. The effects of increasing the entity size in the 1/2 scale calculation by a factor of 15/4 and in the full scale calculation by a factor of 15/2 are small. In the latter problem the delay time for the onset of delivery is reduced by 0.8 seconds and the per cent of injected water that refills the lower plenum is slightly higher. Even less change is seen in the 1/2 scale problem. These results indicate that the flow dynamics are not extremely sensitive to momentum exchange through interfacial drag.

The corresponding curves for the case in which the entity size is determined from the critical Weber number formulation are shown in Fig. 12. Again, the correspondence between these curves and the corresponding ones in Fig. 8 is good. This is consistent with previous observations.[8] Considering that the critical Weber number entity size, Eq. (18), varies both spatially and temporally as $(\vec{u}_1 - \vec{u}_2)^{-2}$, as well as with the transient variation of ρ_2, the similarity of the results of Figs. 8 and 12 indicates that the flow dynamics are not very sensitive to either the form or the magnitude of the momentum exchange function K, Eq. (7), as long as the parameters for the various formulations are within reasonable range.

A comparison of the full-scale curves of Figs. 8, 11, and 12 is shown in Fig. 13. Notice in this figure that the refill curve obtained using the Weber number formulation does not exhibit a pronounced overshoot as seen in the refill curves from the constant entity size calculations. This overshoot results from the sloshing of delivered water from the lower plenum into the downcomer. The spatial dependence of K on relative velocity that is obtained with the Weber number formulation retards this jetting effect.

Additional comparisons of results obtained using a Weber number formulation for entity size and a constant value are given in Table I, runs 1-6.

Wall Heat Transfer Distance, γ. The effect of using Eq. (12) to calculate the depth of penetration of a cooling wave into the wall rather than the formulation given in Ref. 6, Eq. (13), is demonstrated in Figs. 14 and 15. With the use of Eq. (12) the heat transfer from the wall is reduced, so that the water is cooler and there is greater condensation. The effect of this change on the bypass and lower plenum refill curves is slight, as can be seen in Figs. 14 and 15.

Numerical Computations: Effects of Scale, Mesh Resolution, and Two Dimensionality. Computation times for the K-TIF calculations reported in this report varied from 19 to 196 minutes on the CDC 7600 computer. The principal factor affecting the computation time was apparatus scale. For the same mesh resolution, 2/15 scale calculations required 2-3 hours of computation time, 1/2 scale calculations required 35-55 minutes and full scale calculations required 19-27 minutes. The reason for these differences is that we require for numerical accuracy and stability that

$$\delta t < 0.25\ \delta x/u_{max} ,$$

where δt is the computation time increment, δx is the mesh spacing and u_{max} is the maximum velocity magnitude in the system at that time. Since δx is proportional to apparatus scale and u_{max} is approximately the same at all scales because of the steam inflow boundary condition, δt is proportional to scale and the computation time is approximately inversely proportional to scale.

For this reason a full scale calculation was more efficient to use to test the effect of mesh resolution on the flow dynamics. The finite difference spatial resolution in the horizontal and the vertical directions was doubled in this calculation. A comparison of the bypass and refill curves obtained in this calculation and in the calculation with standard resolution is shown in Fig. 16. The high resolution problem was terminated before the lower plenum was 90% full in order to save computer time, but the results shown in the figure provide a clear indication of the effect of increasing the mesh resolution. The time delay for the onset of water delivery to the lower plenum is almost 1 second shorter in the better resolved problem and this time difference is maintained during delivery. Also there is less water bypassed in the calculation with improved resolution. The reason for these differences is the increased momentum exchange through condensation in the problem with coarser resolution resulting in greater water holdup. The magnitude of J, Eq. (3), is approximately the same at the gas-water interface in both cases but, because of the coarseness of the mesh, a greater volume of water is condensed when the mesh spacing is 45 in. rather than 22.5 in.

As indicated in Fig. 4 the lower plenum in these calculations is represented as a two-dimensional extension of the downcomer with volume equal to that of the three-dimensional lower plenum. To test the accuracy of this model we have compared K-TIF results with those obtained in a corresponding calculation using the three-dimensional ZIA code. ZIA is a three dimensional version of K-TIF being developed by F. H. Harlow and A. A. Amsden, and these are preliminary results shown with their permission. In ZIA the fluid dynamics calculation in the downcomer region is virtually identical to that of K-TIF, but the resolution of the lower plenum is fully three dimensional, rather than the two-dimensional K-TIF representation in Fig. 4.

Figure 17 shows bypass and refill curves obtained from a standard K-TIF calculation, a K-TIF calculation that had only one row of cells in the lower

plenum, and the ZIA calculation. The physical parameters were identical in all cases; the only differences were in the computational procedures.

The delay time for the onset of water delivery to the lower plenum is approximately 1.7 seconds greater for the ZIA calculation with a three dimensional lower plenum than for the standard K-TIF calculation with a two-dimensional lower plenum. Also, delivery proceeds more slowly in ZIA, although the per cent of injected water that is delivered to the lower plenum when the lower plenum is 90% full is in good agreement. More water is bypassed through the broken leg in the ZIA calculation than in K-TIF.

The agreement with the ZIA results can be improved if the lower plenum in the K-TIF calculation is restricted to a single row of computation cells rather than the full lower plenum shown in Fig. 4. Then the water bypassed through the broken leg is in better agreement with the ZIA results and the time for the onset of delivery to the lower plenum is in good agreement with ZIA. Of course, after the onset of delivery the water delivery curve is not realistic in this case because of the greatly restricted lower plenum volume.

The explanation of the difference between the time for delivery initiation in ZIA and K-TIF lies in the extra degree of freedom for pressure communication in the lower plenum in the three-dimensional model. The flow field in the lower plenum attempts to adjust to the low pressure at the broken leg in the downcomer by increasing the volume rate of steam flow into the downcomer from below the broken leg and decreasing the steam flow at other azimuthal positions. However, this trend is mitigated by the trend toward pressure equilibration in the lower plenum. But lower plenum pressure equilibration is more complete when the pressure field can communicate radially as in ZIA rather than in an annular geometry as in K-TIF. Thus in K-TIF there is a much greater tendency toward steam flow jetting toward the broken leg than there is in ZIA. As a result there is less momentum transferred from the steam to the water in the regions away from the broken leg in K-TIF so that delivery occurs at an earlier stage of the pressure ramping. This effect can be reduced by confining the steam inflow region to a single row of cells in the lower plenum. Then there is a smaller lower plenum volume in which the flow field can adjust to conditions in the downcomer so that the steam flux into the downcomer is more uniform.

V. EXTENDING SMALL-SCALE EXPERIMENTAL RESULTS TO THE FULL-SCALE REACTOR

One of the primary purposes of this study is to determine how to interpret the results of small scale experiments, such as those performed by Creare, Inc.[1,2] and Battelle Columbus Laboratories,[3-5] in terms of a full-scale reactor. At the present time only tentative statements can be made in this regard, since several factors that effect scaling have not yet been fully examined.

Scaling studies performed at lower plenum pressures that may be appropriate for a full-scale reactor during the bypass and refill stages of a LOCA indicate that flow similarity at all scales is best obtained when the steam inflow velocity is held constant with scale and the water inflow velocity is proportional to scale. However, even with this form for specifying the inflow velocities there were dissimilarities in the flow development. In particular, there was greater momentum exchange from the steam to the water at small scale than at full scale. This discrepancy could probably be removed by decreasing the steam inflow velocity slightly as the scale decreases, e.g.,

$$j_g = \text{constant } (1 + \beta \times \text{scale}) \quad , \tag{19}$$

where the coefficient β is small compared to 1.

Figures 18 and 19 show the predicted correspondence between inflow rates at reduced and full scales in terms of volume rates of flow. The full-scale flow conditions that were examined most extensively in this study, in which the steam inflow velocity was ramped from j_g = 1674 in/sec to zero in 10 sec and the water inflow velocity was held fixed at j_L = 61.5 in/sec, are indicated on these figures. In terms of volume rates of flow these data correspond to steam flow ramped down from 3.1×10^5 ft^3/min and a water flow rate of 8.6×10^4 gal/min. These flow rates were obtained from a system calculation of a LOCA in a Combustion Engineering System 80 reactor. The corresponding flow rates at 1/15 scale are 350 ft^3/min and 25 gal/min, and at 2/15 scale are 5500 ft^3/min and 200 gal/min.

The effect of performing small-scale experiments at reduced lower plenum pressures compared to a full-scale reactor has not been sufficiently examined to make a definitive statement regarding this aspect of small-scale studies. Nor is it yet clear how to specify the deep interior wall tempera-

ture or the ECC subcooling relative to the saturation temperature in view of the greater sensitivity of results to wall heat transfer at small scale. These matters will be the subjects of a continuing study as discussed in the next section.

VI. PLANS FOR FUTURE WORK

At this stage in the scaling study, it has become clear that additional work is needed in several areas, including model development and verification as well as scaling relationships. The K-TIF model development effort will be concentrated on improvements in the phase change model, Eq. (3), and the lower plenum representation. We have observed in this study and previously[10] that the two-phase flow development in the downcomer is very sensitive to variations in the parameters that affect phase change. Therefore, an effort will be made to incorporate greater physical realism in Eq. (3) by investigating the effects of turbulent mixing, steam-water entity size distributions, and material densities on the mass exchange rate. Improvements in the K-TIF lower plenum representation will be designed to make the steam flux from the lower plenum into the downcomer more uniform, thereby increasing the momentum transfer to the water distant from the broken leg.

The K-TIF model should be verified by comparison with small-scale experimental data from Battelle Columbus Laboratories and Creare, Inc. to determine the effects of changes that have been made in the model since the previous comparative study.[10]

Additional effort is required to better understand scaling relationships so that the objectives of this study can be achieved. Progress has been made in determining the effect of inflow boundary conditions on flow similarity at different scales at lower plenum pressures that may be representative of flow in a full scale reactor during the bypass and refill stages of a LOCA. Yet there are discrepancies even in these results that we may be able to remove through modifications such as that shown in Eq. (19). However, the major effort will be concentrated on relating results obtained at smaller lower plenum pressures to those at larger values. These studies will examine the appropriate pressure ramping at different pressure levels, the effect of reduced gas density on momentum transfer and the effects of reduced saturation temperature on phase change and wall heat transfers. Indeed, the appropriate scaling relationship between T_{ECC}, T_s, and

T_{dw} will be the subject of study at all pressure levels in order to account for variations in wall heat transfer with scale.

ACKNOWLEDGMENTS

The author would like to thank F. H. Harlow and A. A. Amsden for providing the results of the ZIA calculation used in Fig. 17.

REFERENCES

1. C. J. Crowley, G. B. Wallis, and D. L. Ludwig, "Steam-Water Interaction in a Scaled Pressurized Water Reactor Downcomer Annulus," Dartmouth College report COO-2294-4 (1974).

2. C. J. Crowley, J. A. Block, and C. N. Cary, "Downcomer Effects in a 1/15-Scale PWR Geometry-Experimental Data Report," Creare, Inc., Hanover, NH, U. S. Nuclear Regulatory Commission report NUREG-281 (1977).

3. R. A. Cudnik, L. J. Flanigan, W. A. Carbiener, W. A. Wooten, and R. S. Denning, "Penetration Behavior in a 1/15-Scale Model of a Four-Loop Pressurized Water Reactor," Battelle Columbus Laboratories report BMI-NUREG-1973 (1977).

4. W. A. Carbiener, R. A. Cudnik, R. C. Dykhuizen, R. S. Denning, L. J. Flanigan, and J. A. Carr, "Steam-Water Mixing and System Hydrodynamics Program, Quarterly Progress Report, April 1, 1977 - June 30, 1977," Battelle Columbus Laboratories report BMI-NUREG-1979 (1977).

5. W. A. Carbiener, R. A. Cudnik, R. C. Dykhuizen, R. S. Denning, L. J. Flanigan, J. A. Carr, "Steam-Water Mixing and System Hydrodynamics Program, Quarterly Progress Report, July 1, 1977 - September 30, 1977," Battelle Columbus Laboratories report BMI-NUREG-1987 (1977).

6. A. A. Amsden, F. H. Harlow, "K-TIF: A Two-Fluid Computer Program for Downcomer Flow Dynamics," Los Alamos Scientific Laboratory report LA-6994 (1978).

7. F. H. Harlow and A. A. Amsden, "Flow of Interpenetrating Material Phases," J. Comp. Phys. 18, 440 (1975).

8. B. J. Daly, "Nuclear Reactor Safety, Quarterly Progress Report, April 1 - June 30, 1977," LA-NUREG-6934-PR, p.22 (1977).

9. H. J. Richter and T. W. Lovell, "The Effect of Scale on Two-Phase Countercurrent Flow Flooding in Vertical Tubes," unnumbered report from Thayer School of Engineering, Dartmouth College (1977).

10. A. A. Amsden, B. J. Daly, and F. H. Harlow, "Nuclear Reactor Safety, Quarterly Progress Report, October 1 - December 31, 1977," LA-7195-PR p.69 (1978).

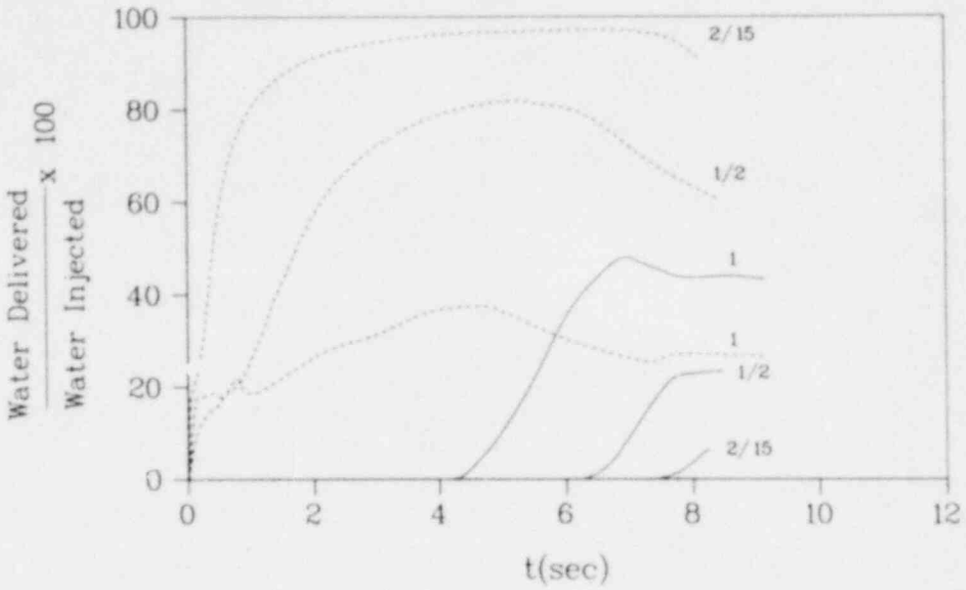

Fig. 5. Runs 9(1), 10(1/2), and 11(2/15). Water delivered to the lower plenum (solid lines) and bypassed through the broken leg (dashed lines) as a percentage of water injected up to that time when the inflow velocities of water and steam are constant with scale.

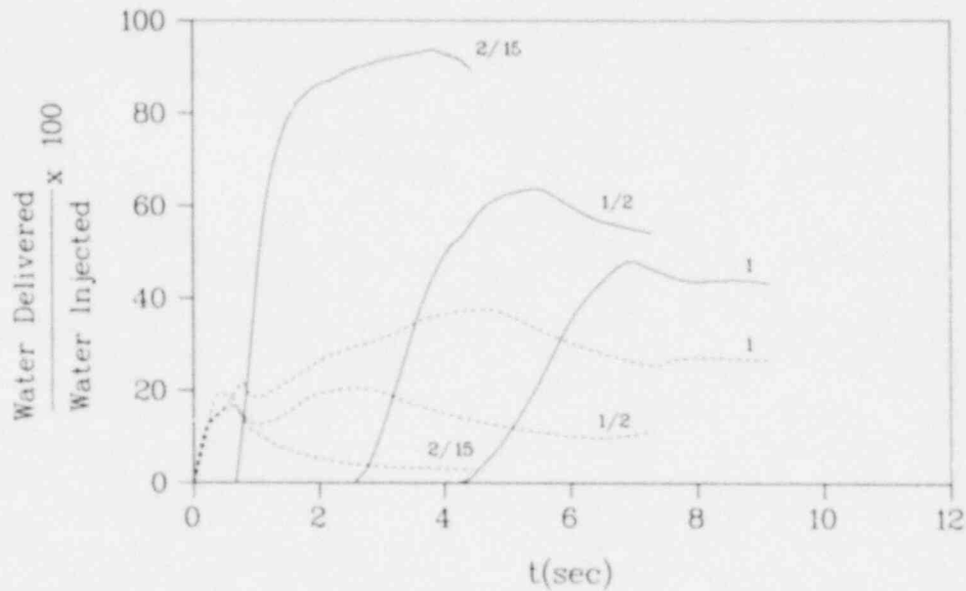

Fig. 6. Runs 9(1), 12(1/2), and 13(2/15). Water delivered to the lower plenum (solid lines) and bypassed through the broken leg (dashed lines) as a percentage of water injected up to that time when the inflow velocities of water and steam are proportional to scale.

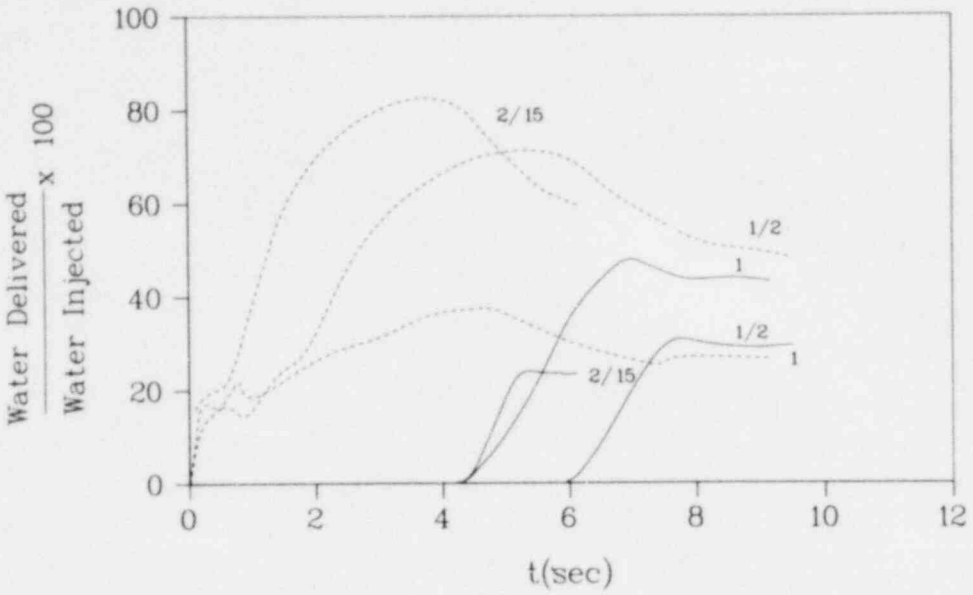

Fig. 7. Runs 9(1), 14(1/2), and 3(2/15). Water delivered to the lower plenum (solid lines) and bypassed through the broken leg (dashed lines) as a percentage of water injected up to that time when the inflow velocities of water and steam are proportional to the square root of the scale.

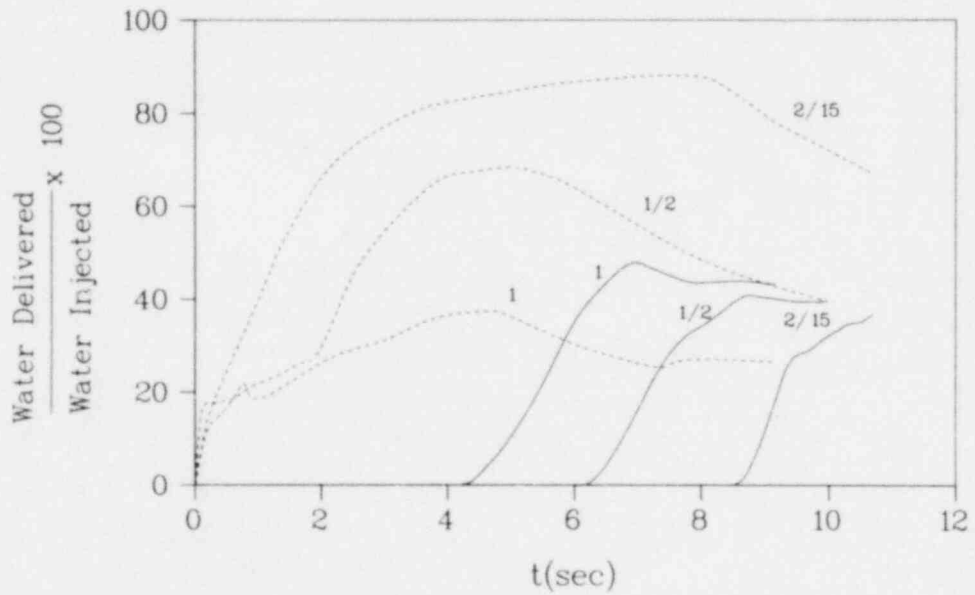

Fig. 8. Runs 9(1), 15(1/2), and 16(2/15). Water delivered to the lower plenum (solid lines) and bypassed through the broken leg (dashed lines) as a percentage of water injected up to that time when the inflow velocity of water is proportional to scale and the inflow velocity of steam is constant with scale.

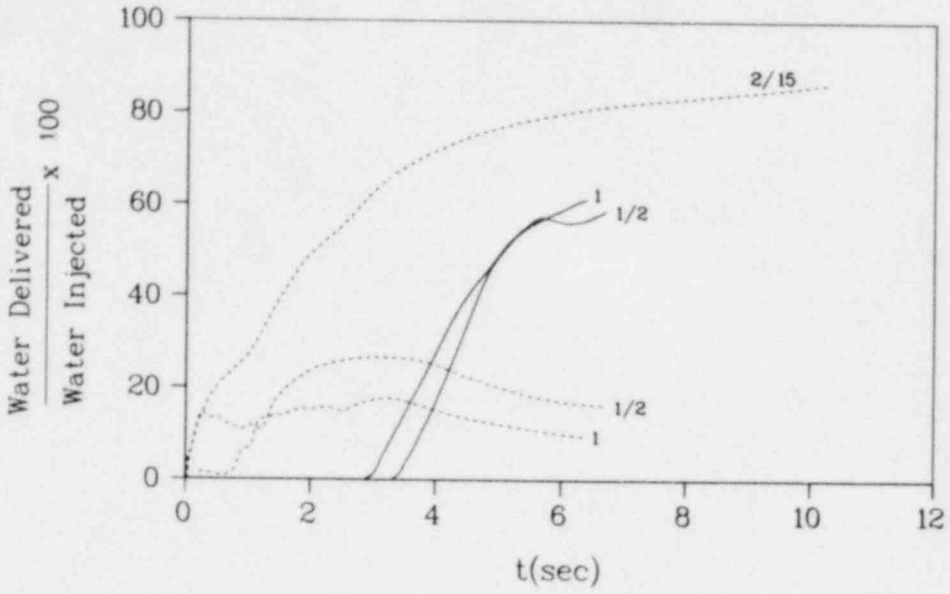

Fig. 9. Runs 27(1), 28(1/2), and 29(2/15). Water delivered to the lower plenum (solid lines) and bypassed through the broken leg (dashed lines) as a percentage of water injected up to that time when the inflow velocity of water is proportional to scale, the inflow velocity of steam is constant with scale and the initial lower plenum pressure is 75 psia. Essentially no water is delivered to the lower plenum at 2/15 scale.

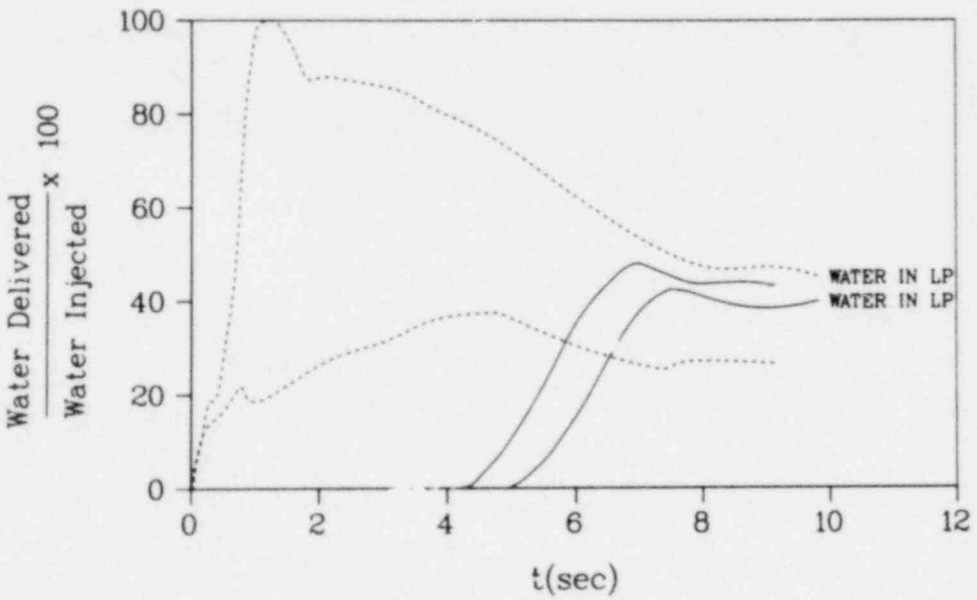

Fig. 10. Full scale runs 9(unmarked) and 26(water in LP). Water delivered to the lower plenum (solid lines) and bypassed through the broken leg (dashed lines) as a percentage of water injected up to that time when the inflow velocity of water is proportional to scale and the inflow velocity of the steam is constant with scale. In run 26 the lower plenum was initially 1/3 full of water.

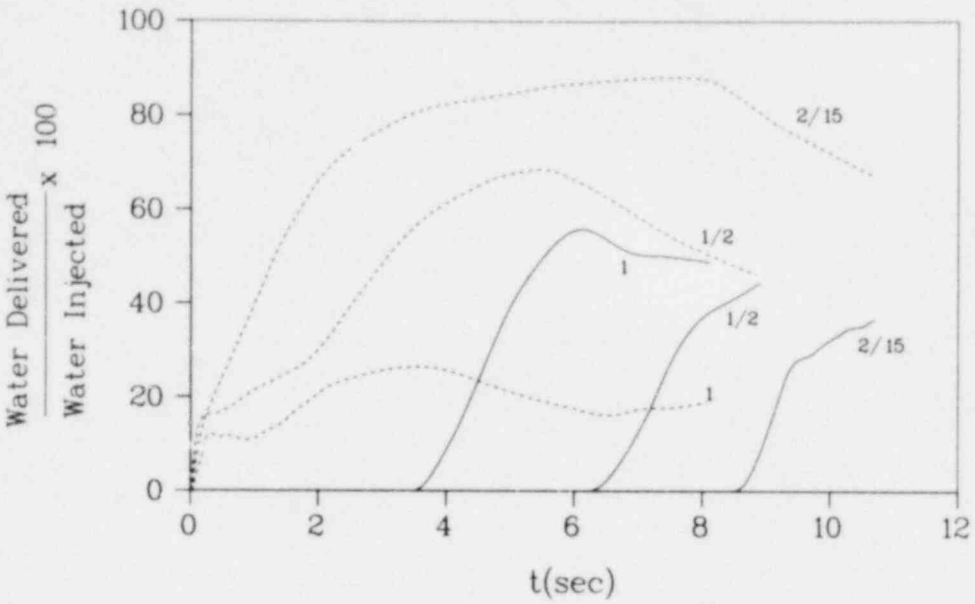

Fig. 11. Runs 21(1), 22(1/2), and 16(2/15). Water delivered to the lower plenum (solid lines) and bypassed through the broken leg (dashed lines) as a percentage of water injected up to that time when the inflow velocity of water is proportional to scale, the inflow velocity of steam is constant with scale and the entity size in Eq. (7) is proportional to scale.

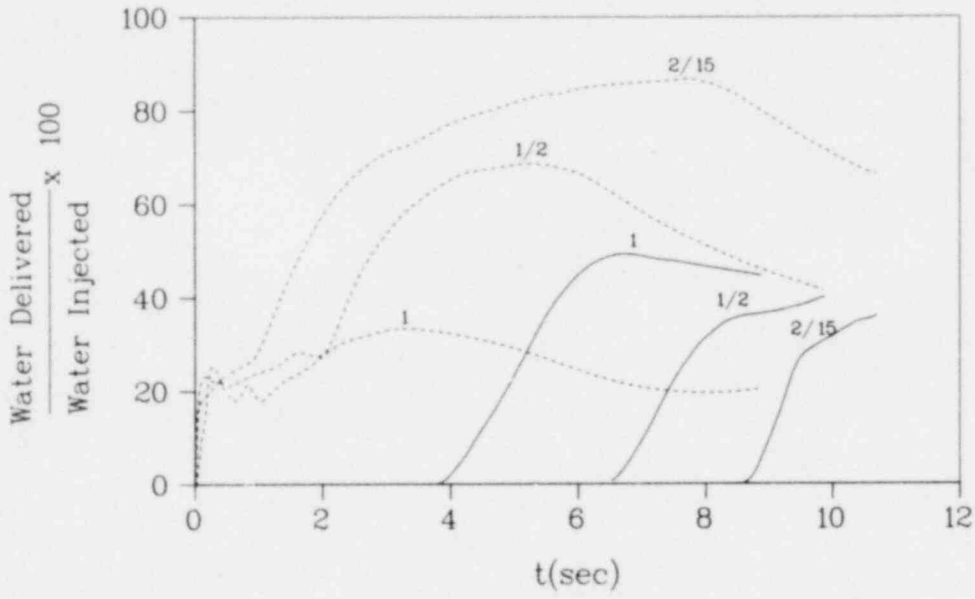

Fig. 12. Runs 18(1), 19(1/2), and 20(2/15). Water delivered to the lower plenum (solid lines) and bypassed through the broken leg (dashed lines) as a percentage of water injected up to that time when the inflow velocity of water is proportional to scale, the inflow velocity of steam is constant with scale and the entity size in Eq. (7) is obtained from a critical Weber number formulation.

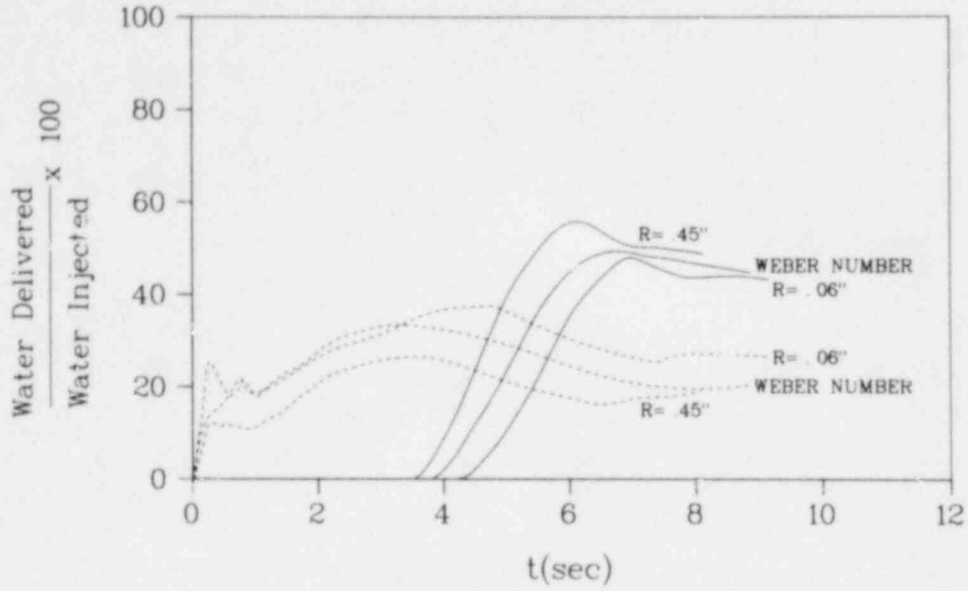

Fig. 13. Full scale runs 9(r = .06"), 18(Weber number), and 21(r = .45"). Water delivered to the lower plenum (solid lines) and bypassed through the broken leg (dashed lines) as a percentage of water injected up to that time when the inflow velocity of water is proportional to scale, the inflow velocity of steam is constant with scale and the entity size in Eq. (7) is determined in three different ways.

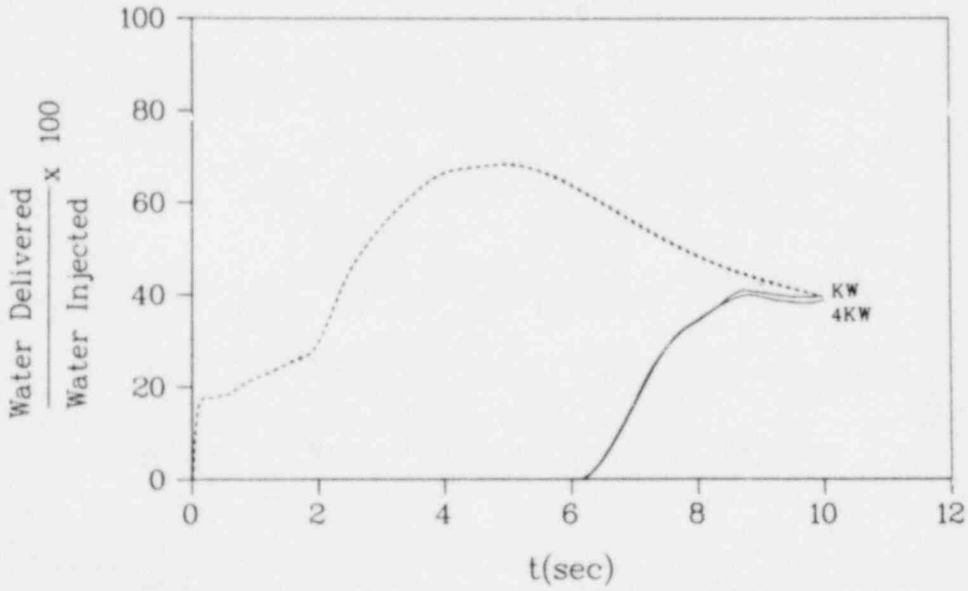

Fig. 14. 1/2 scale runs 15[KW, i.e., Eq. (13)] and 24[4KW, i.e., Eq. (12)]. Water delivered to the lower plenum (solid lines) and bypassed through the broken leg (dashed lines) as a percentage of water injected up to that time when the inflow velocity of water is proportional to scale, the inflow velocity of steam is constant with scale and different rates of penetration of a cooling wave through the walls. There is essentially no difference in the bypass curves.

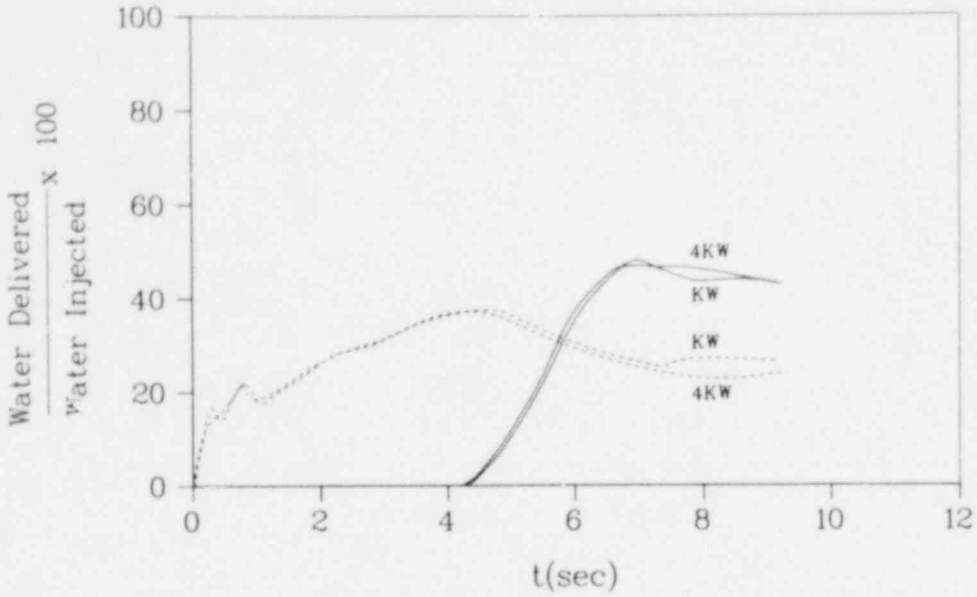

Fig. 15. Full scale runs 9[KW, i.e., Eq. (13)] and 23[4KW, i.e., Eq. (12)]. Water delivered to the lower plenum (solid lines) and bypassed through the broken leg (dashed lines) as a percentage of water injected up to that time when the inflow velocity of water is proportional to scale, the inflow velocity of steam is constant with scale and different rates of penetration of a cooling wave through the walls.

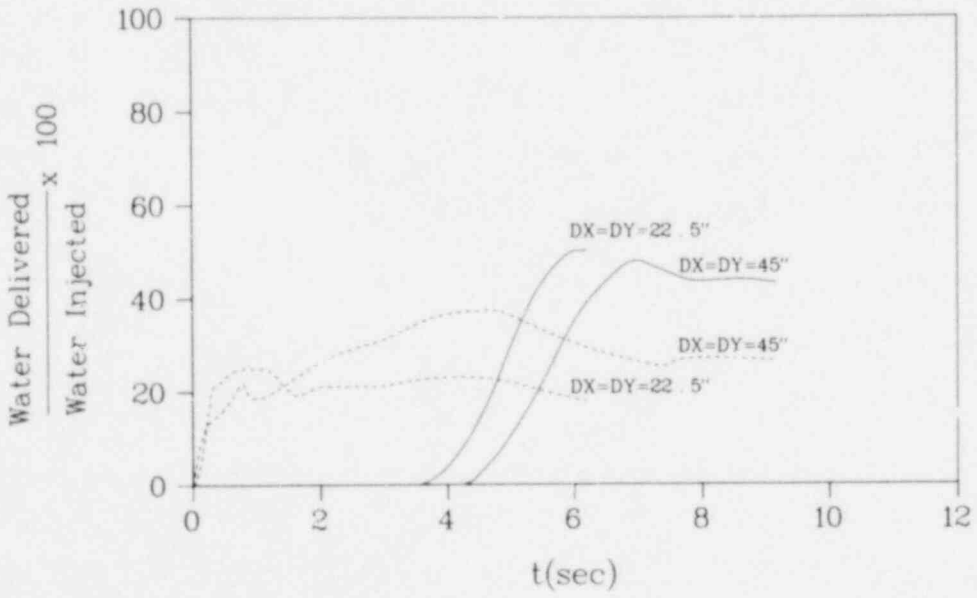

Fig. 16. Full scale runs 9(DX = DY = 45") and 17(DX = DY = 22.5"). Water delivered to the lower plenum (solid lines) and bypassed through the broken leg (dashed lines) as a percentage of water injected up to that time when the inflow velocity of water is proportional to scale, the inflow velocity of steam is constant with scale and using different computation cell sizes.

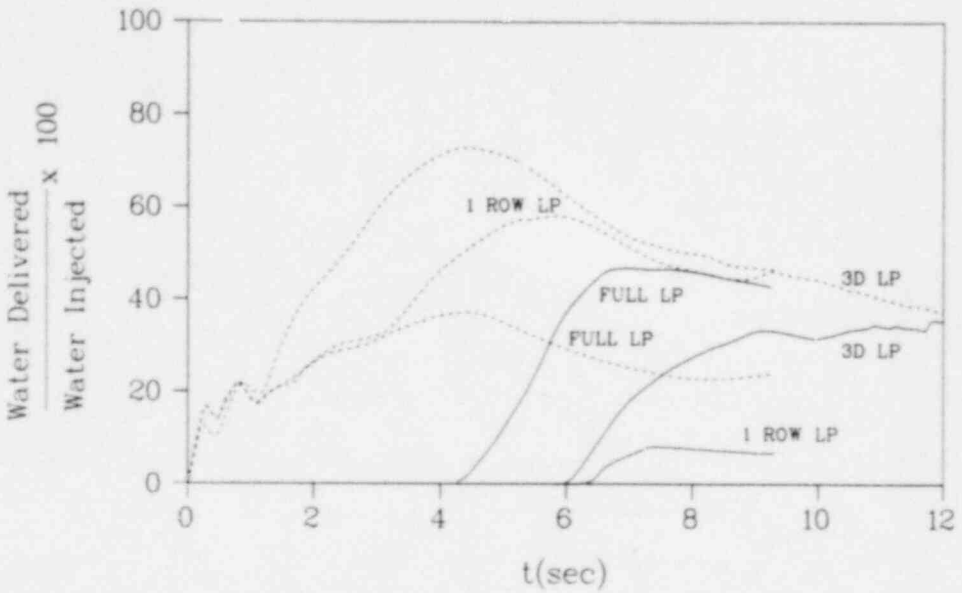

Fig. 17. Full scale runs 23(Full LP), 26(1 row LP), and a ZIA calculation (3D LP). Water delivered to the lower plenum (solid lines) and bypassed through the broken leg (dashed lines) as a percentage of water injected up to that time when the inflow velocity of water is proportional to scale, the inflow velocity of steam is constant with scale and using different lower plenum representations. Full LP corresponds to Fig. 4, 1 row LP indicates a K-TIF calculation in which the lower plenum is represented by a single row of computation cells and 3D LP indicates a ZIA calculation with a fully three-dimensional lower plenum.

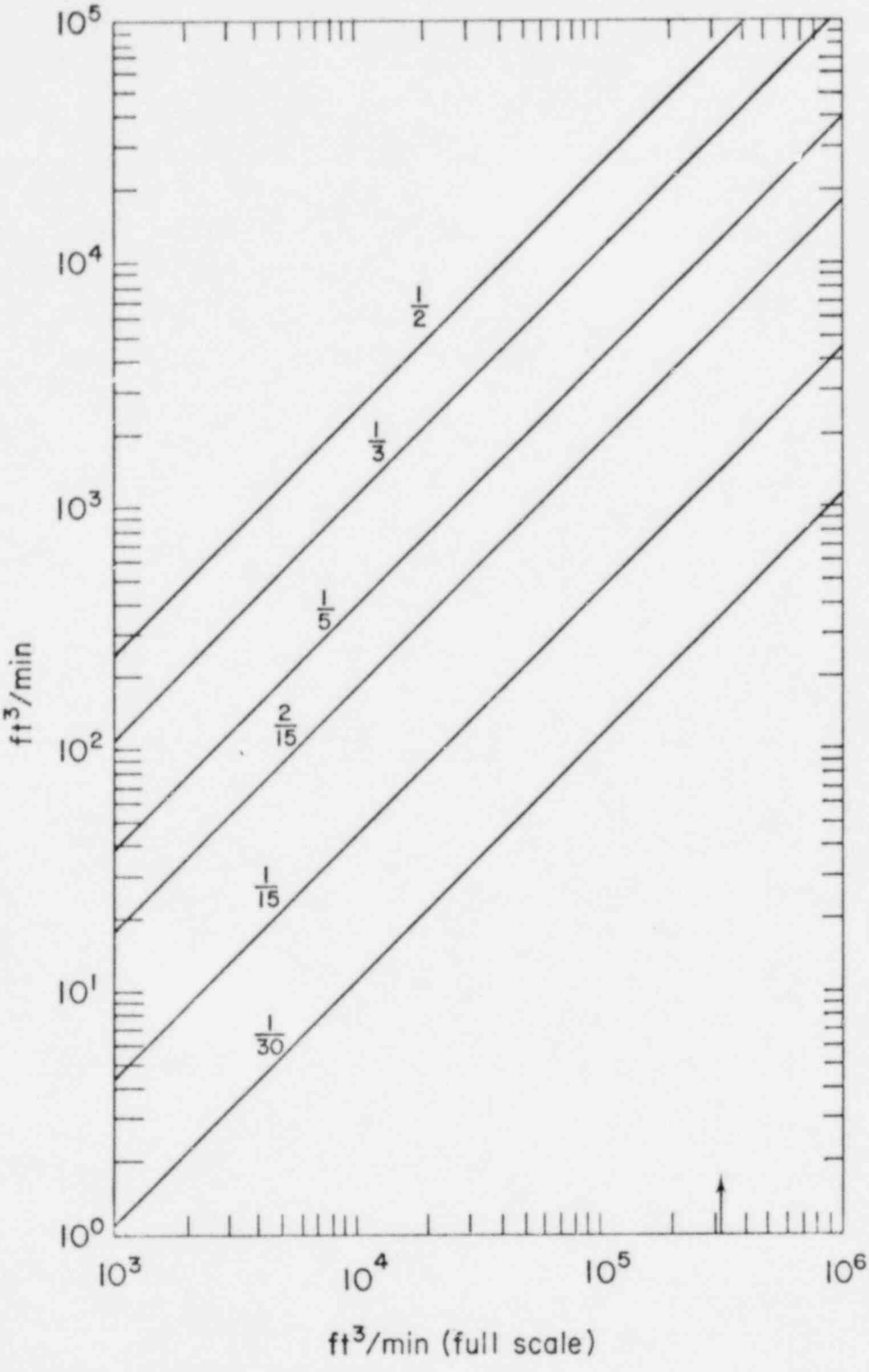

Fig. 18. Correspondence between the volume rate of inflow of steam at various reduced scales and at full scale when the steam inflow velocity is constant with scale. β, Eq. (19), was taken to be zero in obtaining these plots. Arrow shows initial flow rate taken from CE data.

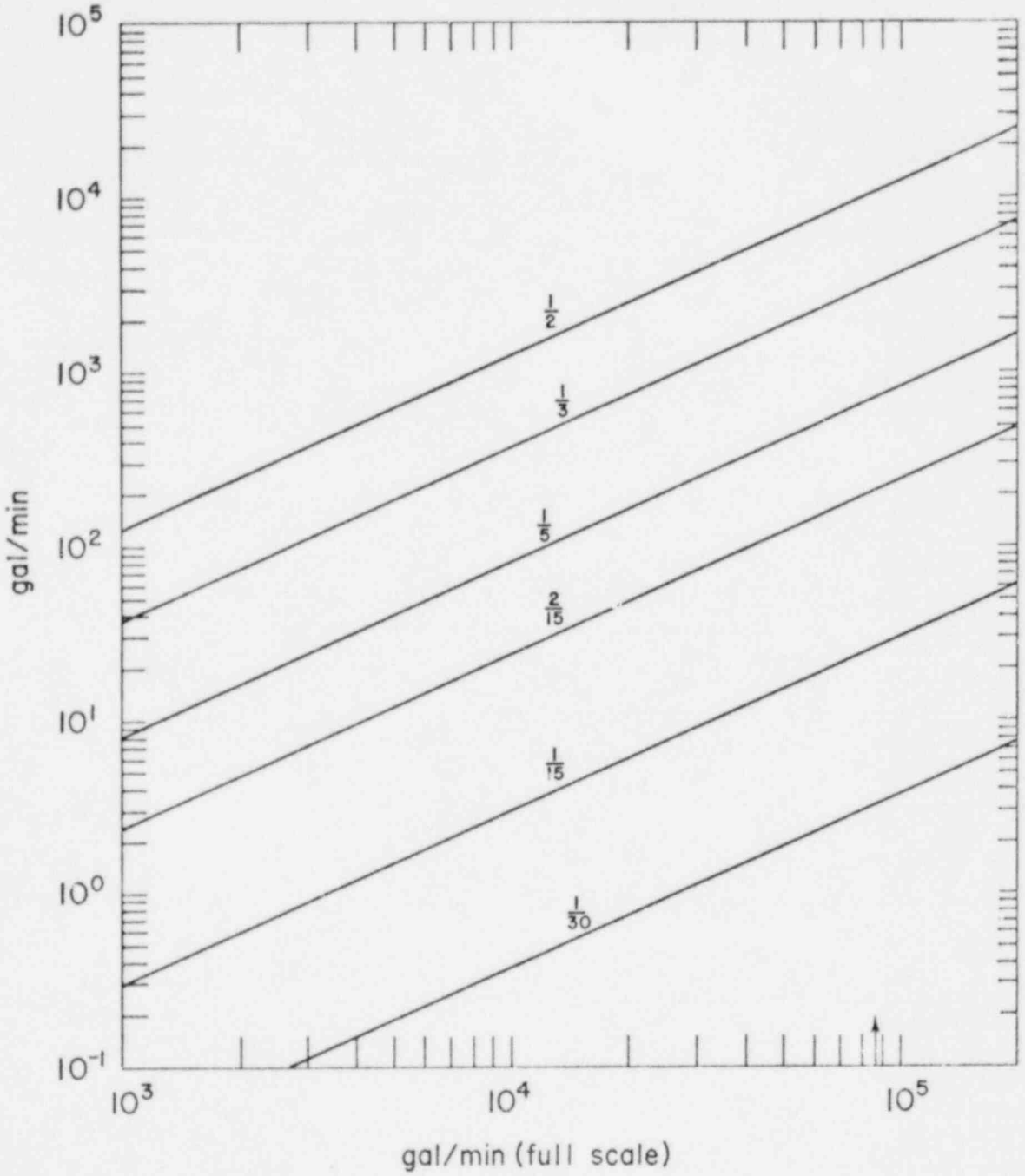

Fig. 19. Correspondence between the volume rate of inflow of water at various reduced scales and at full scale when the water inflow velocity is proportional to scale. Arrow shows flow rate taken from CE data.

☆U.S. GOVERNMENT PRINTING OFFICE: 1978—777-089/122

Available from
US Nuclear Regulatory Commission
Washington, DC 20555

Microfiche	$ 3.00	126-150	7.25	251-275	10.75	376-400	13.00	501-525	15.25
001-025	4.00	151-175	8.00	276-300	11.00	401-425	13.25	526-550	15.50
026-050	4.50	176-200	9.00	301-325	11.75	426-450	14.00	551-575	16.25
051-075	5.25	201-225	9.25	326-350	12.00	451-475	14.50	576-600	16.50
076-100	6.00	226-250	9.50	351-375	12.50	476-500	15.00	601-up	-- 1
101-125	6.50								

1. Add $2.50 for each additional 100-page increment from 601 pages up.

Available from
National Technical Information Service
Springfield, VA 22161